CrossMark

Engineering Styrene Monooxygenase for Biocatalysis: Reductase-Epoxidase Fusion Proteins

Thomas Heine[1] · Kathryn Tucker[2] · Nonye Okonkwo[2] ·
Berhanegebriel Assefa[2] · Catleen Conrad[1] ·
Anika Scholtissek[1] · Michael Schlömann[1] ·
George Gassner[2] (iD) · Dirk Tischler[1,2]

Abstract The enantioselective epoxidation of styrene and related compounds by two-component styrene monooxygenases (SMOs) has targeted these enzymes for development as biocatalysts. In the present work, we prepare genetically engineered fusion proteins that join the C-terminus of the epoxidase (StyA) to the N-terminus of the reductase (StyB) through a linker peptide and demonstrate their utility as biocatalysts in the synthesis of Tyrain purple and other indigoid dyes. A single-vector expression system offers a simplified platform for transformation and expansion of the catalytic function of styrene monooxygenases, and the resulting fusion proteins are self-regulated and couple efficiently NADH oxidation to styrene epoxidation. We find that the reductase domain proceeds through a sequential ternary-complex mechanism at low FAD concentration and a double-displacement mechanism at higher concentrations of FAD. Single-turnover studies indicate an observed rate constant for FAD-to-FAD hydride transfer of ~8 s^{-1}. This step is rate limiting in the styrene epoxidation reaction and helps to ensure that flavin reduction and styrene epoxidation reactions proceed without wasteful side reactions. Comparison of the reductase activity of the fusion proteins with the naturally occurring reductase, SMOB, and N-terminally histidine-tagged reductase, NSMOB, suggests that the observed changes in catalytic mechanism are due in part to an increase in flavin-binding affinity associated with the N-terminal extension of the reductase.

✉ George Gassner
  gassner@sfsu.edu

✉ Dirk Tischler
  dirk.tischler@ioez.tu-freiberg.de

[1] TU Bergakademie Freiberg, Freiberg, Germany

[2] San Francisco State University, San Francisco, CA, USA

Introduction

An array of flavin and iron-containing enzymes has been identified with the ability to catalyze the molecular oxygen-dependent epoxidation of target substrates. The mononuclear iron-containing monooxygenase HppE catalyzes the final step in the biosynthesis of antibiotic fosfomycin [1]. Squalene monooxygenase and zeaxanthin epoxidase catalyze FAD-dependent epoxidations in the biosynthetic pathways for cholesterol and carotenoid pigments [2, 3].

Enzyme-catalyzed epoxidation reactions represent a potentially valuable source of optically active epoxides for the production of pharmaceuticals, agrochemicals, and other biologically active compounds from readily available inexpensive starting materials [4–7]. The enzymatic epoxidation of styrene to styrene-7,8-oxide demonstrated in cytochrome p450 [8], in dinuclear iron-containing methane monooxygenases [9], and in the two-component flavoprotein styrene monooxygenases [4, 10] is of particular interest. Both the versatility and exceptional enantioselectivity of the two-component flavoprotein monooxygenases have led these enzymes to be a primary target for development as commercial catalysts [11, 12].

In *Pseudomonas* sp., the flavoprotein styrene monooxygenase (SMO) converts styrene to (*S*)-styrene oxide in the first step of the styrene catabolic and detoxification pathway [4]. (*S*)-styrene oxide is then isomerized to phenylacetaldehyde by styrene oxide isomerase (SOI) and oxidized to phenylacetic acid by phenylacetaldehyde dehydrogenase (PADH) [13]. Through activation by coenzyme A, phenylacetic acid enters the phenylalanine catabolic pathway and subsequently the TCA cycle [14].

SMO is a two-component flavoprotein composed of an NADH-dependent flavin reductase (styrene monooxygenase reductase (SMOB)) and an FAD-specific styrene epoxidase (SMOA) [15]. SMOB catalyzes the reduction of FAD by hydride transfer from NADH in reaction that is rate limiting in the styrene epoxidation [16]. Following the hydride transfer reaction, reduced FAD leaves the active site of SMOB and binds with high affinity in the active site of SMOA where it reacts rapidly with molecular oxygen to form a stable C(4a)-FAD hydroperoxide. At this point, SMOB, having delivered its FAD to SMOA, is effectively switched off and unable to oxidize NADH and the FAD hydroperoxide in the epoxidase active site is poised to react with styrene [17, 18]. In the presence of styrene, the hydroperoxide intermediate reacts rapidly to yield styrene oxide and a C(4a)-FAD hydroxide intermediate, which in turn dehydrates with the regeneration of oxidized FAD.

The efficiency of this mechanism is dependent on the relative concentrations of the reductase and epoxidase components [19]. As the reductase concentration exceeds that of the epoxidase, the system becomes unregulated and FAD reacts counterproductively with dissolved oxygen to yield hydrogen peroxide and superoxide [19]. It has been possible in some cases to employ SMOs in cell-free and whole-cell-based biocatalytic applications, but the complexity of optimizing two-component enzyme biocatalysts remains a considerable challenge in realizing the versatility and efficiency of these systems [15, 20].

Recently, a SMO from *Rhodococcus opacus* 1CP was discovered, which represents a naturally occurring fusion of reductase and epoxidase activities in a single polypeptide chain [21, 22]. This system was shown to proceed through flavin intermediates similar those of the two-component enzymes from *Pseudomonas* species, but with slower kinetics [23]. This discovery suggested that it might be similarly possible to engineer functional single-

component SMOs by artificially fusing the reductase and epoxidase components of a *Pseudomonas*-system into a single polypeptide [24]. Peptide fusion processes have been previously found in nature and engineered in vitro as means of increasing catalytic activity [25, 26]. Here, we report the characterization of two engineered SMO fusion proteins, compare their catalytic properties to those of the separate reductase and epoxidase components, and evaluate their utility in the small-scale epoxidation of a series of indole derivatives [17–19].

Materials and Methods

Chemicals and Enzymes

Styrene, styrene oxide, indigo, indole, and cofactors were purchased from Sigma-Aldrich and Carl Roth. 4-Methoxyindole, 5-methoxyindole, 6-methoxyindole, 7-methoxyindole, 3-methylindole, 6-chloroindole, methylindole-6-carboxylate, indole-6-carboxylic acid, and 7-azaindole were purchased from TCI. 1-Methylindole, indole-3-acetic acid, and methylindole-5-carboxylate were purchased from ABCR and 6-bromoindole from ChemPur. Enzymes used for cloning purposes were obtained from Thermo Scientific. Oligonucleotides were synthesized by Eurofins MWG Operon.

Bacterial Strains, Plasmids, and Culture Conditions

All bacterial strains and plasmids used in this study are listed in Table 1. *Pseudomonas fluorescens* ST was grown in a desiccator on M9 minimal media plates [27] under oxygen/styrene atmosphere at room temperature [28]. *Escherichia coli* strains were cultivated as described previously [21, 27].

Plasmid Construction and Cloning

SMO genes (Z92524) were amplified by standard polymerase chain reaction (PCR) using DreamTaq DNA polymerase (Thermo Scientific) and appropriate primers (Table 1). The primers allowed changes to be made to terminal gene sequences and for the introduction of linker sequences in the construction of the artificially fused SMO genes. Genomic DNA obtained from *P. fluorescens* ST served as template for PCR reactions. Annealing temperature was optimized for each primer pair as follows in order to obtain respective genes: (i) ST_A_fw/ST_A_rev, 54.8 °C (*styALx*); (ii) ST_fus1B_fw/ST_B_rev, 54.8 °C (*styL1B*); (iii) ST_fus2B_fw/ST_B_rev, 50 °C (*styL2B*); (iv) ST_fus3B_fw/ST_B_rev, 55.6 °C (*styL3B*); and (v) ST_fus4B_fw/ST_B_rev, 53 °C (*styL4B*).

PCR products obtained were purified via agarose gel electrophoresis, and those products of correct size were directly cloned into pJET1.2/blunt yielding pSPfA_B01 and the derivatives pSPfLxB_B01 (x = 1 to 4). Via the restriction sites NdeI and KpnI, the *styA* gene was transferred into pET16bp to provide a first construct pSPfA_P01 for later gene fusion with *styLxBs*. Treatment of pSPfLxB_B01 derivatives with KpnI yielded the fragments *styL1B*, *styL2B*, *styL3B*, and *styL4B*, which were cloned into pSPfA_B01 yielding expression constructs for artificially fused SMOs pSPfALxB_P01. *E. coli* DH5α was used as cloning strain and for plasmid propagation. Expression constructs obtained were finally heat shock transformed into *E. coli* BL21-Gold (DE3) or *E. coli* BL21-Gold (DE3) pLysS for recombinant protein production following the protocol of the manufacturer (Stratagene, Agilent). Sequences of constructed and

Table 1 Strains, plasmids, and primers used in this study

Strain, plasmid, or primer	Relevant characteristic(s)	Source/reference
P. fluorescens ST	Styrene$^+$, Hg$^+$	[50]
E. coli DH5α	F$^-$ φ80d*lacZ* M15 (*lacZYA-argF*)U169 *endA1 recA1 hsdR*17(rK$^-$, mK$^+$) *supE*44 λ$^-$ *thi*-1 *gyrA*96 *relA*1	Gibco-BRL
E. coli BL21(DE3) (pLysS)	*hsdS gal* (λcI*ts*857 *ind*1 Sam7 *nin*5 *lac*UV5-T7 gene 1), pLysS (Cm^R)	Stratagene
E. coli BL21-Gold (DE3)	F$^-$ *ompT hsdS*(rB$^-$ mB$^-$) *dcm$^+$ Tet^r gal endA* The	Stratagene
pJET1.2/blunt	Containing a gene coding for a lethal restriction enzyme, gene disrupting by ligation of a DNA insert into the cloning site possible, T7 promotor	Fermentas
pET16bp	pET16b (Novagen) with additional multi-cloning site, allows expression of recombinant proteins with N-terminal 10× His-tag	[51]
pSPfA_B01	*styA* of *P. fluorescens* ST (PCR-product with primers ST_A_fw/ST_A_rev) cloned in pJET1.2/blunt	This study
pSPfA_P01	*styA* of *P. fluorescens* ST (~1.25 kb NdeI/KpnI-fragment) cloned in pET16bp	This study
pSPfAstop_B01	*styA* of *P. fluorescens* ST (PCR-product with primers ST_A_fw/ST_A_rev_Stop) cloned in pJET1.2/blunt	This study
pSPfAstop_P01	*styA* of *P. fluorescens* ST (~1.25 kb NdeI/NotI fragment) cloned in pET16bp	This study
pSPfL$_x$B_B01	*styB* of *P. fluorescens* ST(PCR-product with different Linkers Lx (1 .. 4) amplified with primers ST_fus1 .. 4B_fw/ST_B_rev) cloned in pJET1.2/blunt	This study
pSPfB_P01	*styB* of *P. fluorescens* ST (~0.5 kb KpnI fragment) cloned in pET16bp	This study
pSPfAL$_x$B_P01	Fusion of *styA* and *styB* with different Linkers Lx (1 .. 4) cloned in pET16bp	This study
ST_A_fw	5′-CATATGAAAAAGCGTATCG-3′; including NdeI site	This study
ST_A_rev_Stop	5′-GCGGCCGCTCAGGCCGCGATAG-3′; including a NotI site	This study
ST_A_rev	5′-GGTACCAGGCCGCGATAGTCGGTG-3′; including KpnI site, removed *styA*-STOP codon	This study
ST_fus1B_fw	5′-GGTACCCATATGACGTTAAAAAAAGATGTG-3′; including KpnI site	This study
ST_fus2B_fw	5′-GGTACCATCATCATCATATGACGTTAAAAAAA GATGTG-3′; including KpnI site, His$_4$-tag	This study
ST_fus3B_fw	5′-GGTACCATGCCGCAGCGATGACGTTAAAAAAA GATGTG-3′; including KpnI site, Ala$_3$-tag	This study
ST_fus4B_fw	5′-GGTACCCATATGGATATCGACTCCACCTGCTTC-3′; including KpnI site, removed of 8 aa at the N-terminus of StyB	This study
ST_B_rev	5′-GGTACCTTAGTTCAGCGGCAACGGCTTG-3′; including KpnI site	This study

cloned genes were verified by automated DNA sequencing (Eurofins MWG Operon). The reductase (N-terminally histidine-tagged version of the styrene monooxygenase reductase (NSMOB)) and epoxidase (N-terminally histidine-tagged epoxidase (NSMOA)) were prepared by using the previously reported pET-28(NSMOB) and pET-28(NSMOA) expression vectors [19].

Whole-Cell Biotransformation of Indole Derivatives

Recombinant StyAL2B was produced by means of the pLysS harboring BL21 derivative as described previously, but using M9 minimal medium with extra thiamine (final concentration 0.01%). After successful expression, the cells were harvested by centrifugation and immediately applied to biotransformations of indole-like substrates (Table 2). A typical assay in a 100-ml Erlenmeyer flask contained 8.5 ml Tris/HCl buffer (50 mM, pH 7.5), 1 ml cell suspension (OD_{600} of 10), and 0.5-ml substrate solution (50 mM Tris/HCl [pH 7.5], 10 mM substrate, 20% DMSO). Cell suspension was tempered for 10 min at 30 °C before adding substrate solution and therewith starting the assay. Biotransformations were carried out for 2 h under constant shaking (150 rpm) at 30 °C. For determination of product formation, 1 ml of the solution was sampled and centrifuged to separate cells and indigoid dye from the aqueous supernatant. Thereafter, the pellet was resuspended in 100 μl DMSO or dimethylformamide (DMF) to dissolve the dyes for spectrophotometric measurements. Conversion of applied indole derivatives by StyAL2B was monitored by formation of the corresponding indigoid dye spectrophotometrically in a range between 200 and 1100 nm (SpectraMax M2e, Software: SoftMax Pro, Molecular Devices).

Preparation of SMO Fusion Proteins

Freshly transformed cells were incubated overnight at 37 °C on Luria broth (LB) agar plates containing 100 μg ml^{-1} ampicillin. Plates used in the production of the pLysS harboring derivative contained in addition 50 μg ml^{-1} chloramphenicol. Colonies containing the protein of interest produced indigo affirming the uptake of the SMO

Table 2 Substrate absorption maxima and reactivity with StyAL2B

Substrate	Conversion	Absorption in DMSO (nm)	Absorption in DMF (nm)	Absorption in H_2O (nm)
Indole	+	620	611	–
1-Methylindole	+	–	–	680
3-Methylindole	–	–	–	–
4-Methoxyindole	+	611	608	–
5-Methoxyindole	+	660	655	–
6-Methoxyindole	+	581	578	–
7-Methoxyindole	+	625	630	–
Indole-2-carboxylic acid	–	–	–	–
Indole-6-carboxylic acid	–	–	–	–
Indole-3-acetic acid	–	–	–	–
Methylindole-5-carboxylate	+	605	–	–
Methylindole-6-carboxylate	–	–	–	–
6-Chloroindole	+	610	602	–
6-Bromoindole	+	610	602	–
7-Azaindole	+	570	–	–
5-Methoxyindole + 6-methoxyindole	+	643	–	–

fusion protein plasmid [29]. Initially, the pLysS system was chosen to express the proteins to allow for greater control over the expression conditions. This particular system lowers background levels of expression pre-induction and was specifically aimed at prevention of inclusion body formation. The DE3 strain was later used in an attempt to increase overall yield of expressed protein.

Starter cultures (5 ml) were grown at 37 °C overnight and expanded to 6×1-l Fernbach flasks containing LB media and 100 μg ml^{-1} ampicillin. After incubating for 30 min with shaking at 250 rpm to initiate growth, the temperature was reduced to 30 °C. The cultures were grown to an optical density at 600 nm of ~0.8 to 1. The flasks were then cooled to 20 °C, and gene expression was induced with 1 mM IPTG overnight at 20 °C. This temperature scheme was determined optimal to reduce the formation of inclusion bodies.

Cells were washed with 50 mM Tris pH 6.8 buffer and collected via centrifugation. The pellet was resuspended on ice in Ni-NTA-FPLC loading buffer (50 mM Tris pH 7.5, 300 mM NaCl, 20 μM FAD) after adding EDTA and PMSF up to 100 μM and 1 mM, respectively. The cells were sonicated on ice for 3 min in 30-s bursts and soluble protein was recovered from the supernatant of high-speed centrifugation (30 min at 50,000×g).

NSMOB and the SMO fusion proteins used in this study were purified by nickel affinity chromatography following a protocol similar to that described previously [19]. Supernatant from the high-speed centrifugation was loaded onto a Sigma His-Select nickel affinity column equilibrated in 50 mM Tris pH 7.5, 300 mM NaCl, and 20 μM FAD. After washing the column isocratically with two column volumes of equilibration buffer, a linear gradient was initiated with the imidazole concentration increasing to 250 mM over the course of three column volumes. Purified protein detected by a post-column UV detector was stored at −20 °C after dilution with glycerol to give a 50% w/w solution.

Sample purity was analyzed by SDS-PAGE with low-range and high-range Bio-Rad molecular weight standards. Protein concentrations were determined using Thermo Scientific Pierce BCA Protein Assay Kit with bovine serum albumin (BSA) standard. Molecular weights and extinction coefficients were estimated using the web-based application ProtParam [30].

The SMOB activity assay used to calculate specific activity is monitored at A_{340} using a quartz microplate and a UV-vis spectrophotometer plate reader. The efficiency of NADH/styrene coupling was determined by simultaneously monitoring absorbance at 340 and 245 nm using the previously described kinetic assay [19]. A Molecular Devices SpectraMax 190 UV plate reader equipped with a quartz microplate was used instead of stopped flow for these measurements [19].

For native SMOB, the absorbance maximum in the visible region shifts from 450 to 456 nm [16]. The extinction coefficient spectrum of FAD bound to the SMO fusion proteins was estimated from Eq. (1). In this calculation, the total concentration of FAD present in the sample was estimated from the total absorbance (A_T) of free and bound FAD in the protein stock solution by using the molar extinction coefficient for bound FAD (11,300 M^{-1} cm^{-1}). The concentration of FAD bound to the linker protein ([FAD]$_{bound}$ parameter) was estimated from the observed absorbance decrease at 450 nm corresponding to the reduction of bound FAD in single-turnover reactions with NADH recorded by using the stopped-flow instrument. The spectrum of the

bound FAD molar extinction coefficients ($\epsilon_{M\lambda}^{\text{bound}}$) was then calculated across the visible wavelength region.

$$\epsilon_{M\lambda}^{\text{bound}} = \frac{A_{\text{T}} - \epsilon_{M\lambda}^{\text{FAD}}[\text{FAD}]_{\text{free}}}{[\text{FAD}]_{\text{bound}}} \qquad (1)$$

Steady-State Kinetic Studies

Kinetic data points were obtained by monitoring the oxidation of NADH at 340 nm. All assays using fusion proteins were recorded by using a Molecular Devices SpectraMax 190 plate reader equipped with a 96-well quartz microplate. Initial reaction rates were computed with the Softmax Pro software. The plate reader was pre-set to 30 °C, and all reagents aside from the enzyme on ice were placed in a water bath set to 30 °C. NSMOB was assayed by using a previously described stopped-flow spectrophotometer at 10 °C [19]. Concentration of NADH ranged from 10 to 400 μM, and FAD concentration ranged from 0.6 to 80 μM where 0.6 μM FAD corresponds to [FAD] brought in from the protein stock. All assays were run in 20 mM MOPSO pH 7 with a final reaction volume of 250 μl. All reagents excluding NADH were premixed in a quartz microplate; the addition of NADH initiated the reactions. Three trials were recorded for each concentration. Initial rate values were recorded in the first 10 s of data collection for StyAL2B and up to 3 min for StyAL1B due to slower velocities. In all cases, less than 5% of the initial NADH concentration was consumed in the time interval used for the initial rate fitting.

Pre-Steady-State Measurements via Stopped-Flow Spectroscopy

Stopped-flow absorbance and fluorescence studies were performed using a single-mixing stopped flow Applied Photophysics instrument previously described [18]. Enzyme was prepared for stopped-flow experiments first by dialysis in 3500 MWCO dialysis tubing for 3 h at 4 °C against 20 mM MOPSO pH 7 buffer to remove glycerol. Before dialysis, the concentration of FAD was brought up to 100 μM to aid in protein stabilization. After dialysis, the tubing was placed directly on a bed of Carbowax PEG 8000 for 3 h at 4 °C to remove water and effectively concentrate the protein. Excess FAD was removed by the addition of 10% v/v charcoal slurry from a preparation of 5% w/w activated charcoal in 20 mM MOPSO buffer pH 7 [31]. After incubation on ice, the charcoal was removed by passage through 0.2-μm Corning Costar cellulose acetate centrifugal filters. The filtrate was immediately placed on ice. This gentle concentration technique was derived after difficulty concentrating protein through other means. A variety of concentration kits including Centriprep-30 concentrators resulted in a loss of activity due to enzyme precipitation. Removal of FAD by gel filtration led to a complete loss of activity. This suggests a more crucial role of FAD on protein stabilization than the native system.

Data Fitting and Analysis

GraphPad Prism 4.0 was used for global fitting of steady-state kinetic studies. The compared model feature of GraphPad Prism was used to analyze which mechanistic model fits the data sets and provided best estimates of binding parameters [32]. Kaleidagraph 4.0 was used for both linear and exponential fittings of stopped-flow data.

Results

Cloning and Expression of SMO Fusion Proteins

Four artificial SMO variants were constructed and successfully cloned into the expression strains. DNA sequencing confirmed the construction, and novel genes allow the production of artificially fused SMOs with StyA at the N-terminus and StyB at the C-terminus. The fused subunits are connected via different linkers expressing certain amino acids (L1 = WYH, L2 = WYHHHH, L3 = WYHAAA, L4 = WYH*), whereas only in case 4, first amino acids of StyB were removed prior linker connection (Fig. S1).

Initially, all four fusion protein constructs were assayed for gene expression. However, only in case of StyAL1B and StyAL2B, soluble and active SMOs were obtained. In the case of StyAL3B and StyAL4B solely insoluble, inactive inclusion bodies were produced (not shown). A variety of media were tested to switch expression into desired soluble form, and in addition, the solubilization and refolding of respective inclusion bodies were tried, but also without any improvement. Thus, we focused on StyAL1B and StyAL2B for biochemical investigations presented here.

Whole-Cell Biotransformation of Indole Derivatives

Recombinant StyAL2B was produced by means of the pLysS harboring BL21 derivative as described previously, but using M9 minimal medium with extra thiamine (final concentration 0.01%). After successful expression, cells were harvested by centrifugation and immediately applied to biotransformations of indole-like substrates (Table 2). A typical assay in a 100-ml Erlenmeyer flask contained 8.5 ml Tris/HCl buffer (50 mM, pH 7.5), 1 ml cell suspension (OD_{600} of 10), and 0.5-ml substrate solution (50 mM Tris/HCl [pH 7.5], 10 mM substrate, 20% DMSO). Cell suspension was tempered for 10 min at 30 °C before adding substrate solution and therewith starting the assay. Biotransformations were carried out for 2 h under constant shaking (150 rpm) at 30 °C. For determination of product formation, 1 ml of the solution was sampled and centrifuged to separate cells and indigoid dye from the aqueous supernatant. Thereafter, the pellet was resuspended in 100 μl DMSO or DMF to dissolve the dyes for spectrophotometric measurements. Conversion of applied indole derivatives by StyAL2B was monitored by formation of the corresponding indigoid dye (Fig. 1) spectropho-tometrically in a range between 200 and 1100 nm (SpectraMax M2e, Software: SoftMax Pro, Molecular Devices).

Fifteen indoles were tested, whereas ten were converted into the corresponding dye (Table 2). It was shown that StyAL2B is able to convert derivatives with substituents at all positions except the 2- and 3-position (Figs. 1 and 2). This corroborates that the substrate is attacked by the SMO at this double bond to form indoxyl, which further undergoes a dimerization to indigo. The color and absorption maximum of the indigoid dye depend on the type and position of the substituents. Interestingly, the often-recorded red by-product and isomer indirubin are not formed by SMO fusion proteins [33]. So, the fusion proteins seem to be highly selective for the production of indigo derivatives.

Whereas all formed dyes were stable in aqueous solution, 7,7′-diazaindigo was readily decomposed in oxygen-saturated solution. As indigo is known to form intramolecular hydro-gen bonds, the nitrogen at the 7-position may destabilize the molecule. In organic solvents, the dyes possess a lower stability and decompose within a few days. Indole-6-carboxylate and
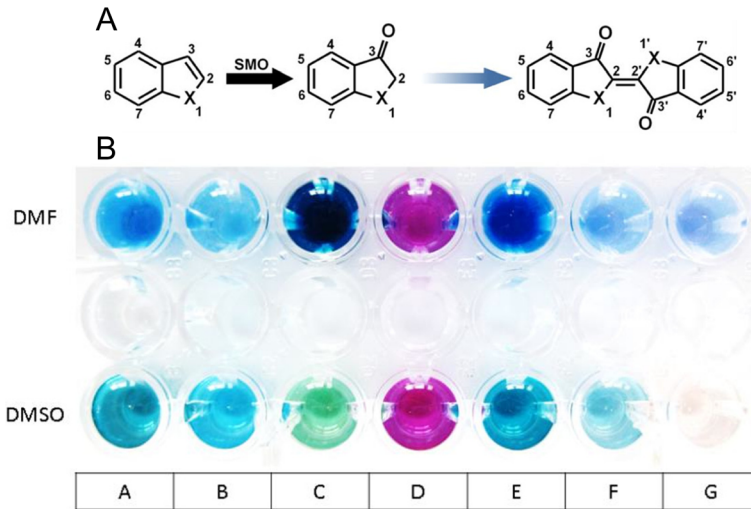
Fig. 1 Biotransformation of indole derivates by SMOs. **a** Indole is converted to indoxyl by SMO activity and spontaneously dimerizes to indigoid dyes. **b** Indigoid dyes formed by StyAL2B: *A* indigo, *B* 4,4′-dimethoxyindigo, *C* 5,5′-dimethoxyindigo, *D* 6,6′-dimethoxyindigo, *E* 7,7′-dimethoxyindigo, *F* 6,6′-dichloroindigo, and *G* 6,6′-dibromoindigo

methyl indole-6-carboxylate were not substrates for StyAL2B, which can be caused by steric hindrance of larger residues at the 6-position. As also shown for 5-methoxyindole and 6-methoxyindole, fusion proteins were able to produce dyes with mixed substituents.

Purification and Recovery of StyAL1B and StyAL2B

Fusion proteins were successfully recovered by means of Ni-NTA-FPLC, but in low concentration (~12–15 mg l^{-1}). Purified protein from the *E. coli* BL21 (DE3) pLysS competent cells gave lower yield, but greater purity than the protein purified from standard *E. coli* BL21 (DE3) cells. Purified fusion proteins were analyzed by SDS-PAGE alongside purified NSMOA and NSMOB fractions for comparison in Fig. 2. In

Fig. 2 FPLC-purified SMO fusion proteins resolved by SDS-PAGE. The contents of each *lane* are as follows: (*1*) low-molecular-weight ladder, (*2*) StyAL1B, (*3*) NSMOA, (*4*) NSMOB, and (*5*) StyAL2B
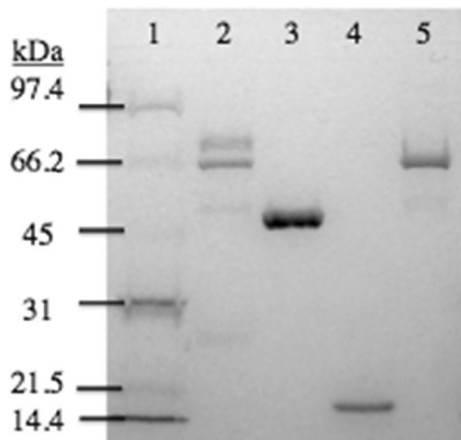
some cases, StyAL1B copurified with a higher-molecular-weight contaminant as shown in lane 2 of the gel. The molecular weights of StyAL1B and StyAL2B estimated from the gel were 65 kDa compared with 65,342 and 65,754 g mol^{-1}, respectively, computed from by using the primary sequences of each fusion protein and the ProtParam program [30]. Total protein-specific activity and stoichiometry of styrene and NADH usage by StyAL1B and StyAL2B are summarized in Table 3.

Figure 3 depicts the best approximation of an extinction coefficient spectrum of StyAL2B computed as explained in experimental methods. This spectrum is compared to the free oxidized FAD extinction coefficient spectrum and the spectrum of the initial stock protein. The slight red shift of maximum around 450 nm of the protein spectrum and of the right shoulder of the peak is indicative of the binding of oxidized FAD to the SMOB domain of the protein [16].

Steady-State Mechanism

It was discovered in evaluating the steady-state kinetic data from StyAL2B that the sequential, two-substrate model with NADH as the leading substrate provided an excellent fit through the data in the low FAD concentration range (0.6–5 μM FAD). At higher concentrations (10–80 μM FAD), the data were better fit by a double-displacement mechanism. The statistical model comparison function built into GraphPad Prism 4.0 was in agreement with this observation. Values of the best fitting steady-state parameters from the reactions of StyAL1B and StyAL2B are compared with wild-type values from the reaction of wild-type SMOB in Table 4.

A model was created that relates the two mechanisms through an oxidized FAD-binding equilibrium (Fig. 4). This model resolves the key FAD and NADH binding activities of the linker proteins proposed in the steady-state mechanism. Under conditions of steady-state turnover, in the absence of styrene, the peroxide intermediate formed in the active site of the epoxidase domain of the linker protein is not very stable, and it rapidly decomposes to yield hydrogen peroxide and oxidized FAD. In the presence of styrene, the peroxide intermediate rapidly reacts to yield styrene oxide.

A steady-state rate equation describing this model is given in Eq. 2 with definitions of the sequential and double-displacement kinetic parameters given in Eqs. 3–6. In Eq. 2, the apparent catalytic rate constants and Michaelis constants for the sequential ternary-complex and double-displacement modes of catalysis are given by $k_{cat}^{app(s)}$, $K_m^{app(s)}$ and $k_{cat}^{app(d)}$, $K_m^{app(d)}$, respectively. The conservations of mass expression (Eq. 7) and rapid

Table 3 Yield and catalytic properties of Ni-NTA-purified SMO fusion proteins

Enzyme	Total recovered protein (mg)[a]	Specific activity (μmol mg^{-1} min^{-1})	[NADH]/[styrene]
StyAL1B	74 ± 4	3.0 ± 0.2	1.0 ± 0.6
StyAL2B	87 ± 4	2.9 ± 0.2	1.0 ± 0.3

[a] Total recovered protein is based on BCA assay. Specific activity assay reaction contained ~50 nM protein, 20 mM MOPSO buffer and 5 μM FAD and initiated with 50 μM NADH and 25 μM styrene. Under these conditions, the epoxidation reactions are rate limited by the preceding reduction

Fig. 3 Electronic spectrum of purified StyAL2B. The spectrum of StyAL2B recorded after PEG concentration and treatment with activated carbon is shown as *dashed lines*. The extinction coefficient spectrum computed as described in the text is shown as a *solid black line*
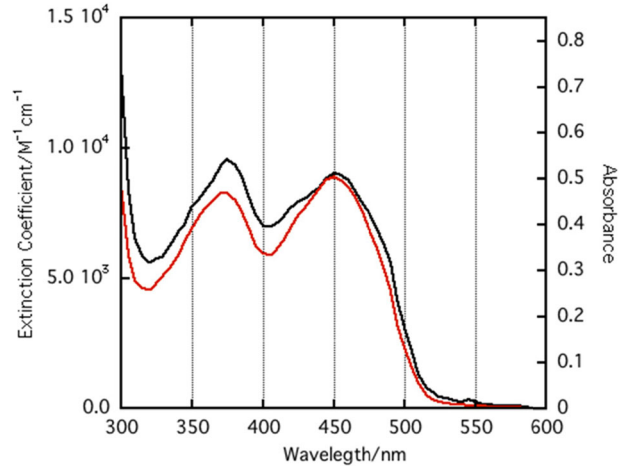
equilibrium approximation were applied in order to derive the quadratic expression defining the binding of oxidized FAD to the apo-linker protein (Eq. 8). In this way, it was possible to globally fit and compute the fraction of the linker protein participating in each mode of catalysis over the complete range of NADH and FAD concentrations.

$$v = \frac{k_{cat}^{app(s)} E_{apo}[\text{NADH}]}{K_m^{app(s)} + [\text{NADH}]} + \frac{k_{cat}^{app(d)} E_{FAD}[\text{NADH}]}{K_m^{app(d)} + [\text{NADH}]} \tag{2}$$

$$K_m^{app(s)} = \frac{K_s^{\text{NADH}} K_m^{\text{FAD}} + K_m^{\text{NADH}}[\text{FAD}]}{K_m^{\text{FAD}} + [\text{FAD}]} \tag{3}$$

Table 4 Comparison of steady-state kinetic parameters of StyAL1B, StyAL2B, SMOB, and NSMOB

Parameter	StyAL1B[a]	StyAL2B[a]	SMOB[b]	NSMOB[c]
$[\text{Enzyme}]_{total}$ (µM)	0.10	0.26	0.01	0.2
$V\text{max}_d$ (µM min^{-1})	11.9 ± 0.9	64.9 ± 1.4	–	38 ± 1.0
$V\text{max}_s$ (µM min^{-1})	17.3 ± 0.7	28.2 ± 0.9	32.4 ± 6.5	–
K_{dFAD} (µM)	47.6 ± 2.0	8.1 ± 1.5	–	–
K_{sNADH} (µM)	45.9 ± 10.8	55.6 ± 13.7	114 ± 41	–
$K_{MFAD(s)}$ (µM)	56.0 ± 2.0	2.1 ± 0.2	86 ± 29	–
$K_{MFAD(d)}$ (µM)	147.3 ± 226.4	14.8 ± 0.9	–	3.7 ± 0.4
$K_{MNADH(s)}$ (µM)	28.3 ± 4.2	27.5 ± 7.1	101 ± 53	–
$K_{MNADH(d)}$ (µM)	64.0 ± 4.0	67.7 ± 2.8	–	5.0 ± 0.1

[a] Values estimated by fitting according to the joint sequential and double-displacement model described (see Fig. 5)

[b] Values from 19 estimated by fitting data with a sequential ternary-complex model with NADH serving as the leading substrate

[c] Kinetic parameters estimated by fitting data with a double-displacement kinetic model
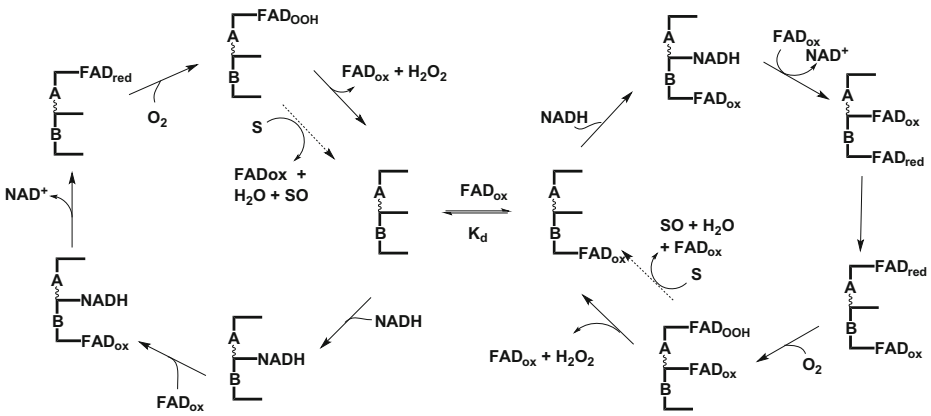
Fig. 4 Interchange of sequential and double-displacement reaction mechanisms. The sequential mechanism (*left*) and double-displacement mechanism (*right*) related through the equilibrium describing the reversible binding of FAD to the apo enzyme. Alternate fates of the flavin peroxide intermediate are shown for the reaction occurring in the absence (*solid arrow*) or absence (*dashed arrow*) of styrene

$$K_m^{\mathrm{app}(d)} = \frac{K_m^{\mathrm{NADH}}[\mathrm{FAD}]}{K_m^{\mathrm{FAD}} + [\mathrm{FAD}]} \tag{4}$$

$$k_{\mathrm{cat}}^{\mathrm{app}(s)} = \frac{k_{\mathrm{cat}}^{s}[\mathrm{FAD}]}{K_m^{\mathrm{FAD}} + [\mathrm{FAD}]} \tag{5}$$

$$k_{\mathrm{cat}}^{\mathrm{app}(d)} = \frac{k_{\mathrm{cat}}^{d}[\mathrm{FAD}]}{K_m^{\mathrm{FAD}} + [\mathrm{FAD}]} \tag{6}$$

$$E_{\mathrm{apo}} = E_t - E_{\mathrm{FAD}} \tag{7}$$

$$E_{\mathrm{FAD}} = \frac{E_t + K_d + [\mathrm{FAD}] - \sqrt{E_t + K_d + [\mathrm{FAD}]^2 - 4E_t[\mathrm{FAD}]}}{2} \tag{8}$$

The model results in a consistent fit through the entire data set for both StyAL1B and StyAL2B shown in Fig. 5. When fitting steady-state data according to this model, the kinetic parameters obtained from the sequential mechanism fits (Table S1) were used as initial fitting parameters. This provided a basis for the fitting algorithm to compute estimates of the remaining kinetic and equilibrium parameters (Table 4). Fluorescence titration was attempted in order to estimate directly the equilibrium dissociation constant of oxidized FAD; however, due to instability of the fusion proteins in the presence of low [FAD], this technique was unsuccessful. It was possible to directly estimate the equilibrium dissociation constant of ~70 nM for FAD binding to NSMOB by fluorescence-monitored titration (Fig. S3).

Fig. 5 Steady-state kinetics of the reaction of SMO fusion proteins with NADH and FAD. Initial rates from the reaction of StyAL1B and StyAL2B at a range of concentrations of NADH and FAD are shown in plot **a** and plot **b**, respectively. FAD concentrations of 0.6, 2.5, 5, 10, 20, 40, 60, and 80 μM were evaluated at each concentration of NADH. Each plotted point represents the mean value of three to five independent determinations. *Y-error bars* correspond to one standard deviation. *Lines* passing through the data correspond to the best global fit computed according to the model presented in the text
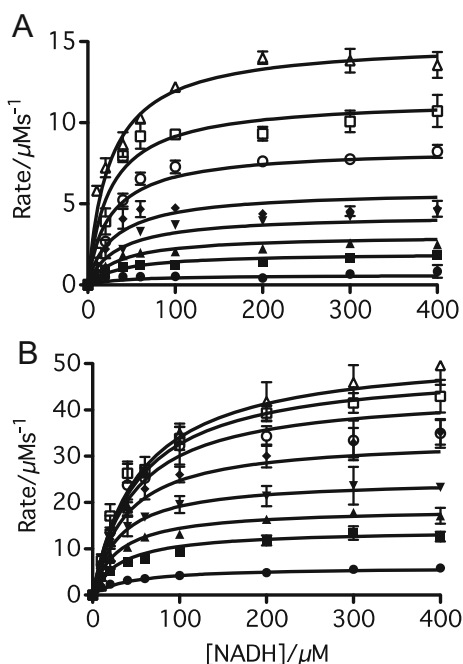
This proposed steady-state model represents the behavior of the StyAL2B system quite well. In the case of the StyAL1B data set, determination of the preferential mechanisms at low and high [FAD] ranges is less definitive due to the relatively high standard deviation of initial fitting parameters obtained from the individual mechanisms (supplemental information Table S1).

The parameters obtained in Table 4 represent the best fitting parameters for the SMO fusion proteins after extensive analysis. It is noted that alternate fits are possible and the numerical values are considered to represent only the approximate range of the actual values. Kinetic parameters for native SMOB, which proceeds exclusively through a sequential ternary-complex mechanism [19, 34], and NSMOB, which proceeds exclusively through a double-displacement mechanism, are included for comparison.

Stopped-Flow Studies of the Reaction of StyAL1B and StyAL2B with NADH

The kinetics of the FAD reduction and styrene epoxidation reactions were observed by absorbance and fluorescence measurements after reacting the fusion proteins with NADH, styrene, and oxygen in a series of stopped flow experiments. These reactions were conducted at 15 °C by rapidly mixing solutions of enzyme equilibrated with FAD with solutions containing NADH in the presence or absence of styrene or benzene. Results summarizing rate constants calculated from fitting these data are compared with NSMOB and those previously reported for NSMOA and SMOB in Table 5.

The kinetics of flavin reduction by StyAL1B and StyAL2B monitored by stopped-flow absorbance spectroscopy are compared in Fig. 6a. The reduction of FAD occurs as a first-order decay observed at 450 nm with a rate constant of 8.2 ± 0.1 s^{-1} for StyAL2B and 7.7 ± 0.3 s^{-1} for StyAL1B. After this initial pre-steady single-turnover reaction, the enzyme enters into a

Table 5 Comparison of rates determined from pre-steady-state analysis and fitting of plots in Figs. 5, 6, and 7

Reaction	StyAL1B	StyAL2B	NSMOB + NSMOA	SMOB + NSMOA
NADH → FAD Hydride transfer (s^{-1})	ND	ND	57 ± 3	50.0 ± 1.7
FAD → FAD Hydride transfer (s^{-1})	7.7 ± 0.3	8.2 ± 0.1	7.9 ± 0.1	–
Styrene epoxidation (s^{-1})	ND	6.00 ± 0.08	3.7 ± 0.5	49.7 ± 0.3

period of steady-state turnover until running out of the limiting reagent, NADH. This complete reaction profile is shown for StyAL2B in Fig. 6b.

The FAD C-(4a) hydroperoxide intermediate of NSMOA can be stabilized by including benzene as a non-reactive styrene analog [18]. A similar phenomenon is observed when StyAL2B is reacted with NADH and benzene under aerobic reaction conditions (Fig. 6b). After the pre-steady-state flavin reduction step (first second of reaction time), the reaction including benzene remains in steady state for a significantly longer time than the benzene-excluding reaction (compare time periods between 1 and 5 s). Once the reductase domain has consumed all available NADH, FAD is observed to reoxidize to a lesser extent in the reaction that included benzene by comparison with the same reaction in the absence of benzene (compare reactions in the 5–10-s time period).

Fig. 6 Kinetics of the aerobic reaction of StyAL1B and StyAL2B with NADH and FAD in the absence of styrene. **a** Reactions of 1.5 μM StyAL1B with 25 μM FAD and 200 μM NADH (*squares*) and 15 μM StyAL2B with 33 μM FAD and 250 μM NADH (*circles*) monitored by absorbance at 450 nm for 1 s. **b** Comparison of the reaction of ~17 μM StyAL2B with 200 μM NADH and 80 μM FAD in the presence (*triangles*) and absence (*circles*) of 5 mM benzene
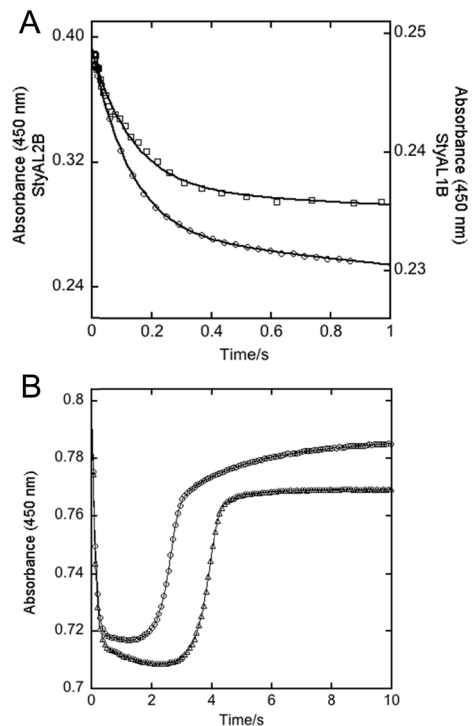
Fig. 7 Comparison of the FAD reduction and styrene epoxidation reactions of the two-component SMO (NSMOA/NSMOB) and StyLA2B in 20 mM aerobic MOPSO buffer at pH 7. **a** Reaction of 5.6 μM NSMOB and 15 μM NSMOA 30 μM FAD, 250 μM NADH, and 250 μM styrene. The kinetics of NADH oxidation was monitored by absorbance at 340 nm (*circles*) and styrene epoxidation reaction by fluorescence emission at 520 nm (*squares*) with excitation at 410 nm. **b** Reaction of 15 μM StyAL2B, 30 μM FAD, 250 μM NADH, and 220 μM styrene monitored by fluorescence emission at 520 nm. Kinetics of FAD reduction were observed using an excitation wavelength of 450 nm (*circles*). The kinetics of styrene epoxidation (*squares*) were observed using an excitation wavelength of 410 nm. *Lines* passing through the data points represent the best exponential fits through these data with the results of the kinetic fitting presented in Table 5
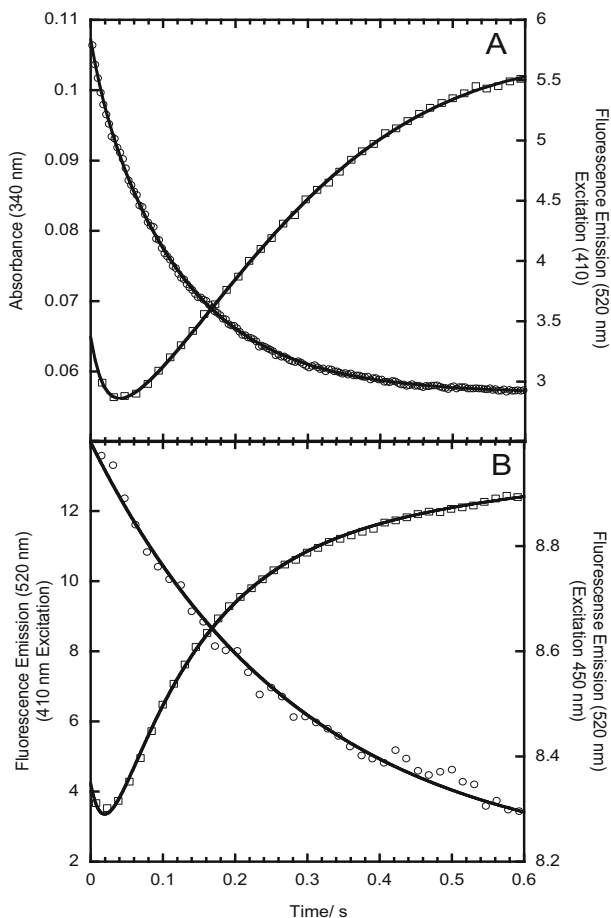
Comparison of the Styrene Epoxidation Reactions of StyAL2B and NSMOB/NSMOA

Data from single-turnover reactions of StyAL2B and NSMOB/NSMOA with NADH oxygen and styrene are presented in Fig. 7. The experimental approach was similar to that used previously to characterize the kinetics of flavin reduction and styrene epoxidation catalyzed by native SMOB and NSMOA [16]. Reaction rate constants determined by exponential fitting are presented in Table 5.

In the reaction of the two-component SMO recorded by stopped-flow absorbance spectroscopy, the kinetics of hydride transfer from NADH to oxidized FAD ($k \sim 57$ s^{-1}) are followed by the kinetics of hydride transfer from the tightly bound coenzyme FAD to substrate FAD ($k \sim 7.9$ s^{-1}). The kinetics of the styrene epoxidation reaction ($k \sim 3.7$ s^{-1}) were recorded by stopped-flow fluorescence spectroscopy by using an excitation wavelength of 410 nm and emission wavelength of 520 nm (Fig. 7a). Similar studies were completed with StyAL1B and StyAL2B. In the case of the linker proteins, the FAD reduction reaction was observed by stopped-flow fluorescence measurement as a single kinetic phase ($k \sim 8$ s^{-1}). The following styrene epoxidation reaction occurs with a rate constant of about 6 s^{-1}.

Discussion

The two-component E-class SMOs have demonstrated value in enzymatic synthesis of enantiopure styrene oxide [34]. Further work based on active site mutagenesis and directed evolution indicates the potential to further improve the catalytic activity and substrate specificity of SMO [35–38]. In the present work, we have characterized a pair of genetically engineered fusion proteins, which coordinate flavin reduction and styrene epoxidation activities in the same polypeptide with the goal or streamlining the work required to engineer, express, and implement catalytic variants of SMO for applications in biocatalysis. This approach has proven to be successful in the engineering of the naturally occurring cytochrome p450 fusion protein, BM3, and is further inspired by the recent discovery of the naturally occurring SMO fusion protein StyA2B [21, 39].

SMOs show potential for development as biocatalysts for the synthesis of indigoid dyes, a class of compounds, are of interest in pharmaceutical [38, 40–44] and industrial applications [45, 46]. However, the uncoupling of the reduction and epoxidation reactions in coexpression systems engaging two-component SMOs results in the release of H_2O_2, which has a negative effect on the stability of indigoid dyes [47]. The ease of fusion protein expression and their highly coordinated epoxidation and reduction reactions are desirable attributes for the production high-quality dye products. Here, we demonstrate the utility SMO fusion proteins as biocatalysts for the synthesis of the transformation of a broad range of substituted indoles to indigoid chromophores including a valuable dye, Tyrian purple. These compounds can be synthesized in pure form economically in an eco-friendly process by using these engineered SMO fusion proteins.

Considerations in the Design and Function of SMO Fusion Proteins

Joining reductase and epoxidase components of SMO via a peptide tether has the potential to introduce strain and further interfere with the assembly, stability, and catalytic activity of artificially linked fusion proteins. Overexpression of the reductase component of SMO results primarily in the formation of inclusion bodies that must be refolded to yield active protein [19, 34]. In addition, the native SMO assembles interact in catalysis as dimers. The fusion proteins must similarly adopt functional quaternary structure. Despite the intrinsic challenges to assembly, it has proven possible to create viable engineered fusion proteins with desirable characteristics.

In this study, two of the engineered fusion proteins, StyAL1B and StyAL2B, were recovered as soluble and catalytically active enzymes. These proteins were found to work well in whole-cell biocatalytic applications and can be recovered in pure form. Expression of the fusion proteins from *E. coli* BL21(DE3) cells at 37 °C, conditions found to be optimal for the production of native and N-terminally histidine-tagged epoxidase component of SMO, primarily yielded protein that partitioned into inclusion bodies. In order to recover these proteins in soluble and active form, it was necessary to induce protein expression in *E. coli* BL21(DE3) pLysS cells at low temperature over a longer time period than used for the separate, wild-type, or N-terminally histidine-tagged components of SMO. Addition of oxidized FAD in buffers used in the purification further stabilizes the fusion proteins during purification and recovery.

It has been demonstrated that protein-protein interaction is an important aspect of the mechanism of FAD recycling between the reductase and epoxidase [16, 19], and it was

previously shown that the reductase and epoxidase are each dimers in solution [34]. However, no structural data are available to suggest exactly how the reductase and epoxidase dimers bind to each other in catalysis. The quaternary structures of the StyAL1B and StyAL2B fusion proteins are expected to be constrained by the amino acid tethers that link the N-terminus of the reductase and C-terminus of the monooxygenase domains. Favorable interfacial interactions that stabilize the dimeric assembly of reductase and monooxygenase of the two-component SMO are expected to similarly favor the assembly of reductase and epoxidase domains of the fusion proteins. The linker regions are thought to be long enough to allow the formation of dimeric fusion protein structures. However, higher-order assemblies involving even numbers of fusion protein monomers are also possible. Mechanistic features of the engineered fusion proteins are largely conserved when compared with the two-component SMO. This suggests that the quaternary assembly of the fusion protein subunits is similar to that adopted by the two-component SMOs. Further structural studies will be needed to resolve whether alternate catalytically functional quaternary structures have been adopted.

Steady-State Mechanism

In our evaluation of the reaction of the fusion proteins, we find that the predominant steady-state mechanism is dependent on FAD concentration. At low FAD concentration, the reaction kinetics of the reductase domains are best modeled by the sequential mechanism previously shown to describe the behavior of the wild-type reductase [19, 34]. At higher FAD concentrations, the steady-state mechanism shifts to a double-displacement reaction. We were able to successfully fit the full range of steady-state data from the linker proteins by using a composite model joining the sequential and double-displacement mechanisms though an oxidized FAD binding equilibrium.

The type of steady-state mechanism employed is dependent in part on the extension of the N-terminus of SMOB. Native SMOB, which proceeds exclusively through a sequential ternary-complex mechanism, binds oxidized FAD with Kd = 1.2 μM at 25 °C [16]. In the present work, we find that extending the N-terminus of SMOB by 20 amino acids in the N-terminally histidine-tagged protein, NSMOB, results in a 17-fold increase in FAD binding affinity (Kd ~70 nM) and a double-displacement reaction mechanism.

Following this trend, we hypothesized that the fusion proteins might bind FAD with an equilibrium dissociation constant bracketed by native and NSMOB, but we have been unable to measure the value of this parameter due to the instability of the apo-proteins. Our best estimates of the Kd values for oxidized FAD binding to the fusion proteins come from steady-state kinetic analysis (Table 4), but the Kd values returned from these models represent the binding affinity of FAD to catalytically active states of the enzymes, which may be different than those present under equilibrium conditions. In addition, our kinetic model assumes that FAD binding occurs as a rapid equilibrium in catalysis and, for this reason, has the potential to significantly underestimate the FAD-binding affinity at thermodynamic equilibrium. On this basis, we view that the Kd values returned from steady-state kinetic fitting as a lower limit for the binding affinity of FAD to the fusion proteins.

Coupling of NADH and Styrene Oxidation Reactions

In the single-turnover mechanism of SMO, FAD is first reduced by hydride transfer from NADH in the active site of SMOB. Reduced FAD is then transferred to the active site of

NSMOA where it reacts with oxygen to form a relatively stable C-(4a) hydroperoxide intermediate. At this point, the reductase is depleted of FAD and effectively prevented from further turnover. Oxidized FAD is regenerated and returned to SMOB only after NSMOA completes the styrene epoxidation reaction or in the absence of styrene as the C(4a)-hydroperoxide intermediate decomposes with the elimination of hydrogen peroxide [16]. This carefully coordinated FAD exchange reaction allows for efficient coupling of the NADH oxidation and styrene epoxidation reactions.

In the reaction of wild-type SMO, the kinetics of styrene epoxidation occur rapidly (k ~104 s^{-1}) compared with the rate of flavin reduction (k ~50 s^{-1}) such that the styrene epoxidation reaction is limited by the rate of flavin reduction [16]. This configuration helps to minimize the accumulation-reduced FAD in solution where it can react unproductively with oxygen as a free species.

Single-turnover studies of the fusion proteins and NSMOB indicate that they reduce substrate FAD with a rate constant of about 8 s^{-1}. This FAD-to-FAD hydride transfer step, which occurs only in the double-displacement reaction, limits the kinetics of the epoxidation reactions catalyzed by both StyAL2B (k ~6 s^{-1}) and the two-component SMO composed of NSMOB and NSMOA (k ~3.7 s^{-1}).

The ternary-complex flavin reduction mechanism employed by the native reductase, SMOB, plays an important role in the regulation of SMO. Once the reduced FAD product is transferred from SMOB to the NSMOA, it has been proposed that the apo-reductase remains associated with the epoxidase through the course of the epoxidation reaction [16]. During this time, the reductase is effectively switched off until the NSMOA-catalyzed epoxidation is completed. The return transfer of oxidized FAD from NSMOA to SMOB provides the reductase with the substrate that it needs to continue the reduction reaction.

In the double-displacement reaction catalyzed by NSMOB and the reductase domain of the fusion proteins, coenzyme FAD remains bound in the active site and bulk flavin reduction is slowed but not switched off by the transfer of reduced FAD to the epoxidase. The catalytic efficiency of the epoxidation reaction of the fusion proteins seems to be rooted primarily in their rate of the flavin reduction reaction, which is slow compared with the kinetics of styrene epoxidation.

The C(4a)-FAD peroxide intermediate is greatly stabilized when benzene is included in the single-turnover reaction of NSMOA [18]. In the presence of benzene, the steady-state turnover of NADH by StyAL2B continues but at a diminished rate. Stabilization of the peroxide intermediate by benzene is also observed in the post-steady-state reoxidation phase that occurs as NADH is depleted as the limiting reagent. The absorbance remains constant, indicating that the previously observed ability of the substrate analog, benzene, to effectively stabilize the flavin peroxide intermediate of NSMOA is retained in the epoxidase domain of the fusion proteins [18].

Fusion Proteins as Efficient Biocatalysts

Fusing the two components of the native system results in two catalytic entities within one polypeptide. Connecting the two subunits forces a 1:1 ratio of reductase to epoxidase. This ratio helps to circumvent the uncoupling that can occur when the reductase concentration exceeds that of the epoxidase in the native two-component system [19]. In the presence of excess FAD, StyAL2B reacts through a double-displacement mechanism that results in the reduction of FAD faster than it can be used by the epoxidase. Coordinated, stoichiometric

oxidation of NADH and styrene by StyAL2B occurs at low FAD concentration, and StyAL2B represents an efficient biocatalyst with potential for the production of valuable optically active chiral compounds.

Active site mutations aimed at engineering an active site that can accommodate a larger range of substrates in conjunction with a more efficient fusion protein result in a novel much more valuable biocatalyst. The fusion proteins evaluated here can be further combined with previous efforts aimed at accommodation of a broader substrate spectrum to allow for the efficient biocatalysis of a larger range of styrene analogs in the synthesis of valuable epoxides [36, 38, 48, 49].

References

1. Higgins, L. J., Yan, F., Liu, P., Liu, H. W., & Drennan, C. L. (2005). Structural insight into antibiotic fosfomycin biosynthesis by a mononuclear iron enzyme. *Nature, 437*, 838–844.
2. Laden, B. P., Tang, Y., & Porter, T. D. (2000). Cloning, heterologous expression, and enzymological characterization of human squalene monooxygenase. *Archives of Biochemistry and Biophysics., 374*, 381–388.
3. Hieber, A. D., Bugos, R. C., & Yamamoto, H. Y. (2000). Plant lipocalins: violaxanthin de-epoxidase and zeaxanthin epoxidase. *Biochimica et Biophysica Acta, 1482*, 84–91.
4. Hartmans, S., van der Werf, M. J., & de Bont, J. A. (1990). Bacterial degradation of styrene involving a novel flavin adenine dinucleotide-dependent styrene monooxygenase. *Applied and Environmental Microbiology, 56*, 1347–1351.
5. Archelas, A., & Furstoss, R. (1997). Synthesis of enantiopure epoxides through biocatalytic approaches. *Annual Review of Microbiology, 51*, 491–525.
6. Choi, W. J. (2009). Biotechnological production of enantiopure epoxides by enzymatic kinetic resolution. *Applied microbiology and biotechnology., 84*, 239–247.
7. Lin, H., Liu, J. Y., Wang, H. B., Ahmed, A. A., & Wu, Z. L. (2011). Biocatalysis as an alternative for the production of chiral epoxides: a comparative review. *Journal of Molecular Catalysis B: Enzymatic., 72*, 77–89.
8. Fukami, T., Katoh, M., Yamazaki, H., Yokoi, T., & Nakajima, M. (2008). Human cytochrome P450 2A13 efficiently metabolizes chemicals in air pollutants: naphthalene, styrene, and toluene. *Chemical Research in Toxicology, 21*, 720–725.
9. Green, J., & Dalton, H. (1989). A stopped-flow kinetic study of soluble methane mono-oxygenase from Methylococcus capsulatus (Bath). *The Biochemical Journal, 259*, 167–172.
10. Thibodeaux, C. J., Chang, W. C., & Liu, H. W. (2012). Enzymatic chemistry of cyclopropane, epoxide, and aziridine biosynthesis. *Chemical Reviews, 112*, 1681–1709.
11. van Berkel, W. J., Kamerbeek, N. M., & Fraaije, M. W. (2006). Flavoprotein monooxygenases, a diverse class of oxidative biocatalysts. *Journal of Biotechnology, 124*, 670–689.
12. Huijbers, M. M., Montersino, S., Westphal, A. H., Tischler, D., & van Berkel, W. J. (2014). Flavin dependent monooxygenases. *Archives of Biochemistry and Biophysics., 544C*, 2–17.
13. Panke, S., Witholt, B., Schmid, A., & Wubbolts, M. G. (1998). Towards a biocatalyst for (S)-styrene oxide production: characterization of the styrene degradation pathway of Pseudomonas sp. strain VLB120. *Applied and Environmental Microbiology, 64*, 2032–2043.
14. Teufel, R., Mascaraque, V., Ismail, W., Voss, M., Perera, J., Eisenreich, W., Haehnel, W., & Fuchs, G. (2010). Bacterial phenylalanine and phenylacetate catabolic pathway revealed. *Proceedings of the National Academy of Sciences of the United States of America, 107*, 14390–14395.
15. Montersino, S., Tischler, D., Gassner, G. T., & van Berkel, W. J. (2011). Catalytic and structural features of flavoprotein hydroxylases and epoxidases. *Advanced Synthesis and Catalysis, 353*, 2301–2319.
16. Morrison, E., Kantz, A., Gassner, G. T., & Sazinsky, M. H. (2013). Structure and mechanism of styrene monooxygenase reductase: new insight into the FAD-transfer reaction. *Biochemistry, 52*, 6063–6075.

17. Ukaegbu, U. E., Kantz, A., Beaton, M., Gassner, G. T., & Rosenzweig, A. C. (2010). Structure and ligand binding properties of the epoxidase component of styrene monooxygenase. *Biochemistry, 49*, 1678–1688.
18. Kantz, A., & Gassner, G. T. (2011). Nature of the reaction intermediates in the flavin adenine dinucleotide-dependent epoxidation mechanism of styrene monooxygenase. *Biochemistry, 50*, 523–532.
19. Kantz, A., Chin, F., Nallamothu, N., Nguyen, T., & Gassner, G. T. (2005). Mechanism of flavin transfer and oxygen activation by the two-component flavoenzyme styrene monooxygenase. *Archives of Biochemistry and Biophysics., 442*, 102–116.
20. Bae, J. W., Doo, E. H., Shin, S. H., Lee, S. G., Jeong, Y. J., Park, J. B., & Park, S. (2010). Development of a recombinant *Escherichia coli*-based biocatalyst to enable high styrene epoxidation activity with high product yield on energy source. *Process Biochemistry., 45*, 147–152.
21. Tischler, D., Eulberg, D., Lakner, S., Kaschabek, S. R., van Berkel, W. J., & Schlomann, M. (2009). Identification of a novel self-sufficient styrene monooxygenase from Rhodococcus opacus 1CP. *Journal of Bacteriology, 191*, 4996–5009.
22. Tischler, D., Kermer, R., Groning, J. A., Kaschabek, S. R., van Berkel, W. J., & Schlomann, M. (2010). StyA1 and StyA2B from Rhodococcus opacus 1CP: a multifunctional styrene monooxygenase system. *Journal of Bacteriology, 192*, 5220–5227.
23. Tischler, D., Schlomann, M., van Berkel, W. J., & Gassner, G. T. (2013). FAD C(4a)-hydroxide stabilized in a naturally fused styrene monooxygenase. *FEBS letters., 587*, 3848–3852.
24. Tischler, D., Groning, J. A., Kaschabek, S. R., & Schlomann, M. (2012). One-component styrene monooxygenases: an evolutionary view on a rare class of flavoproteins. *Applied Biochemistry and Biotechnology, 167*, 931–944.
25. Munro, A. W., Leys, D. G., McLean, K. J., Marshall, K. R., Ost, T. W., Daff, S., Miles, C. S., Chapman, S. K., Lysek, D. A., Moser, C. C., Page, C. C., & Dutton, P. L. (2002). P450 BM3: the very model of a modern flavocytochrome. *Trends in Biochemical Sciences, 27*, 250–257.
26. Jawanda, N., Ahmed, K., & Tu, S. C. (2008). Vibrio harveyi flavin reductase–luciferase fusion protein mimics a single-component bifunctional monooxygenase. *Biochemistry, 47*, 368–377.
27. Sambrook, J., & Russell, D. W. (2001). *Molecular cloning; a laboratory manual* (3rd ed.). Cold Spring Harbor, NY: Cold Spring Harbor Laboratory Press.
28. Oelschlagel, M., Groning, J. A., Tischler, D., Kaschabek, S. R., & Schlomann, M. (2012). Styrene oxide isomerase of Rhodococcus opacus 1CP, a highly stable and considerably active enzyme. *Applied and Environmental Microbiology, 78*, 4330–4337.
29. O'Connor, K. E., & Hartmans, S. (1998). Indigo formation by aromatic hydrocarbon-degrading bacteria. *Biotechnology Letters., 20*, 219–233.
30. Gasteiger E., Hoogland C., Gattiker A., Duvaud S., Wilkins M. R., Appel R. D. et al. (2005). Protein identification and analysis tools on the ExPASy server. In J. M. Walker (Ed.), *The Proteomics Protocols Handbook* (pp. 571–607). Humana Press.
31. Chen, R. F. (1967). Removal of fatty acids from serum albumin by charcoal treatment. *The Journal of Biological Chemistry, 242*, 173–181.
32. Motulsky, H. J., & Christopoulos, A. (2003). *Fitting models to biological data using linear and nonlinear regression*. San Diego: GraphPad Software Inc..
33. Choi, H. S., Kim, J. K., Cho, E. H., Kim, Y. C., Kim, J. I., & Kim, S. W. (2003). A novel flavin-containing monooxygenase from Methylophaga sp strain SK1 and its indigo synthesis in *Escherichia coli*. *Biochemical and biophysical research communications., 306*, 930–936.
34. Otto, K., Hofstetter, K., Rothlisberger, M., Witholt, B., & Schmid, A. (2004). Biochemical characterization of StyAB from Pseudomonas sp. strain VLB120 as a two-component flavin-diffusible monooxygenase. *Journal of Bacteriology, 186*, 5292–5302.
35. Qaed, A. A., Lin, H., Tang, D. F., & Wu, Z. L. (2011). Rational design of styrene monooxygenase mutants with altered substrate preference. *Biotechnology Letters, 33*, 611–616.
36. Lin, H., Qiao, J., Liu, Y., & Wu, Z. L. (2010). Styrene monooxygenase from Pseudomonas sp. LQ26 catalyzes the asymmetric epoxidation of both conjugated and unconjugated alkenes. *Journal of Molecular Catalysis B: Enzymatic., 67*, 236–241.
37. Lin, H., Liu, Y., & Wu, Z. L. (2011). Highly diastereo- and enantio-selective epoxidation of secondary allylic alcohols catalyzed by styrene monooxygenase. *Chemical Communications (Cambridge, England), 47*, 2610–2612.
38. Lin, H., Tang, D. F., Ahmed, A. A., Liu, Y., & Wu, Z. L. (2012). Mutations at the putative active cavity of styrene monooxygenase: enhanced activity and reversed enantioselectivity. *Journal of Biotechnology, 161*, 235–241.
39. De Mot, R., & Parret, A. H. (2002). A novel class of self-sufficient cytochrome P450 monooxygenases in prokaryotes. *Trends in Microbiology, 10*, 502–508.
40. Kapadia, G. J., Tokuda, H., Sridhar, R., Balasubramanian, V., Takayasu, J., Bu, P., Enjo, F., Takasaki, M., Konoshima, T., & Nishino, H. (1998). Cancer chemopreventive activity of synthetic colorants used in foods, pharmaceuticals and cosmetic preparations. *Cancer Letters, 129*, 87–95.

41. Hössel, R. (1999a). *Synthese von Derivaten des Indirubins und Untersuchungen zur Mechanismsaufklärung ihrer antineoplastischen Wirkung*. Kaiserslautern: Universität Kaiserslautern.
42. Guengerich, F. P., Sorrells, J. L., Schmitt, S., Krauser, J. A., Aryal, P., & Meijer, L. (2004). Generation of new protein kinase inhibitors utilizing cytochrome p450 mutant enzymes for indigoid synthesis. *Journal of Medicinal Chemistry, 47*, 3236–3241.
43. Guengerich, P. F., Martin, M. V., McCormick, W. A., Nguyenb, L. P., Glover, E., & Bradfield, C. A. (2004). Aryl hydrocarbon receptor response to indigoids in vitro and in vivo. *Archives of Biochemistry and Biophysics., 423*, 309–316.
44. Wu, Z. L., Aryal, P., Lozach, O., Meijer, L., & Guengerich, F. P. (2005). Biosynthesis of new indigoid inhibitors of protein kinases using recombinant cytochrome P450 2A6. *Chemistry & Biodiversity, 2*, 51–65.
45. Harrer, R. (2012). Indigo auf Speicherchips. *Chemie in userer Zeit, 46*, 136.
46. Uehara, K., Takagishi, K., & Tanaka, M. (1987). The Al/Indigo/Au photovoltaic cell. *Solar Cells., 22*, 295–301.
47. Lüttke, W., & Hunsdiecker, D. (1966). Theoretische und spetroskopische Untersuchungen an Indigofarbstoffen, IV. Substituenteneffekt am Indigo: Die Darstellung des 5.5′-und 6.6′-Diaza-indigos. *Chemische Berichte, 99*, 2146–2154.
48. Gursky, L. J., Nikodinovic-Runic, J., Feenstra, K. A., & O'Connor, K. E. (2010). In vitro evolution of styrene monooxygenase from Pseudomonas putida CA-3 for improved epoxide synthesis. *Applied microbiology and biotechnology., 85*, 995–1004.
49. Nikodinovic-Runic, J., Coulombel, L., Francuski, D., Sharma, N. D., Boyd, D. R., Ferrall, R. M., & O'Connor, K. E. (2013). The oxidation of alkylaryl sulfides and benzo[b]thiophenes by *Escherichia coli* cells expressing wild-type and engineered styrene monooxygenase from Pseudomonas putida CA-3. *Applied microbiology and biotechnology., 97*, 4849–4858.
50. Baggi, G., Boga, M. M., Catelani, D., Galli, E., & Treccani, V. (1983). Styrene catabolism by a strain of *Pseudomonas fluorescens. Systematic and Applied Microbiology, 4*, 141–147.
51. Wehmeier Personal Communication.